Spread of correlations in strongly disordered lattice systems with long-range coupling

Karol Kawa [*] and Paweł Machnikowski [†]
Department of Theoretical Physics, Wrocław University of Science and Technology, 50-370 Wrocław, Poland

(Received 5 July 2021; revised 28 April 2022; accepted 2 May 2022; published 18 May 2022)

We investigate the spread of correlations in a one-dimensional lattice system with high on-site energy disorder and long-range couplings with a power-law dependence on the distance ($\propto r^{-\mu}$). The increase in correlation between the initially quenched node and a given node exhibits three phases: quadratic in time, linear in time, and saturation. No further evolution is observed in the long time regime. We find an approximate solution of the model valid in the limit of strong disorder and reproduce the results of numerical simulations with analytical formulas. We also find the time needed to reach a given correlation value as a measure of the propagation speed. Because of the triple-phase evolution of the correlation function, the propagation changes its time dependence. In the particular case of $\mu = 1$, the propagation starts as a ballistic motion and then, at a certain crossover time, turns into standard diffusion.

DOI: 10.1103/PhysRevB.105.184204

I. INTRODUCTION

In relativistic physics, information cannot propagate faster than the speed of light c. The upper limit for the propagation of information is determined by the so-called light cone, which means that the minimum time for sending information between points distant by r is $t = r/c$.

Nonrelativistic quantum theory does not impose any limitation on the speed of information propagation in the quantum system explicitly. However, an upper limit of the speed at which quantum information can be transmitted can be induced by finite-range interactions. Indeed, Lieb and Robinson [1,2] proved the existence of such a limit for a lattice model with finite-range interactions (decreasing at least exponentially). They showed that for times $t < r/v$, the correlation between nodes distant by r decreases exponentially.

The presence of this Lieb-Robinson boundary has been observed in many theoretical and experimental studies [3–12], e.g., the first experimental evidence was achieved in the system of a one-dimensional quantum gas trapped in an optical lattice [5]. Those authors focused on the evolution of the two-point correlation function after the local quench, tracking the time of the maximum correlation for successive atoms. In this way the maximum velocity of the correlation propagation was demonstrated.

While the Lieb-Robinson bound applies to locally interacting systems, much recent effort has been devoted to proving the existence of a similar limit in lattice systems with long-range interactions, decreasing with distance according to the power law $\propto 1/r^{\mu}$ [8,9,13–17]. The first mathematical evidence for the existence of a linear light cone in systems with long-range interactions was given in Ref. [14]. In one spatial dimension and for $\mu > 3$, they show that the time required to correlate distant atoms increases at least linearly with distance. In Ref. [13], the authors provide mathematical evidence that a linear light cone occurs in d-dimensional long-range interacting systems for $\mu > 2d + 1$ (which determines the exponent greater than 3 in one dimension). However, other studies [15,18] show that beyond that regime either a subpolynomial, polynomial, or superpolynomial light cone can occur, e.g., while the boundary is calculated using different definitions of operator norms.

Apart from the nature of the coupling, an important factor determining the properties of lattice systems is disorder. After the seminal paper of Anderson [19] the focus shifted to tight-binding-like models with nearest-neighbor couplings, where important formal results concerning localization and transport were obtained [20,21]. More recently, much interest was devoted to models of uncorrelated diagonal disorder with long-range power-law hopping [22–24], where transport properties were characterized via an analysis of the localization of states depending on the coupling exponent and disorder strength [22,24].

In this paper we aim at merging these two aspects and describe the correlation dynamics in long-range-coupled strongly disordered systems, that is, in the parameter range opposite to the disorder-free systems studied so far. We present a complete theory of correlation dynamics in a one-dimensional chain of spins with power-law couplings and strongly disordered on-site energies, based on approximate analytical solutions validated by numerical simulations. Long-range couplings allow the initially quenched spin to communicate with distant spins immediately; hence we observe an immediate spreading of correlations. In contrast to disorder-free systems [13,14], the correlation transfer in the strong disorder limit is driven by such direct interactions with remote but energetically resonant sites. We establish a universal triple-phase dynamics of the correlation growth at a given site. First, the correlations increase like a square of time, and then at a certain instant of time there is a change to a growth directly

[*] karol.kawa@pwr.edu.pl
[†] pawel.machnikowski@pwr.edu.pl

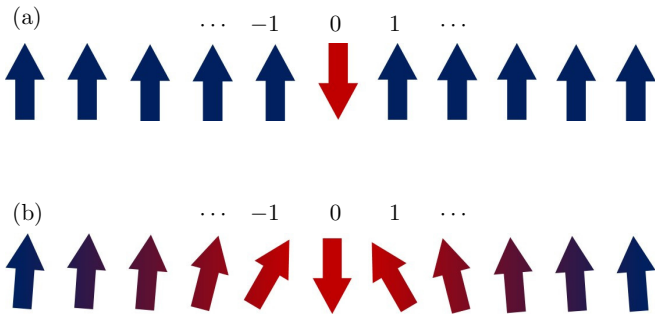

FIG. 1. Schematically illustrated physical system: a chain of uniformly distributed spins with periodic boundary conditions. (a) When one of the spins is rotated (single local quench), interactions occur in the system. (b) The rotated central spin pulls on the other spins, causing excitation to move through the system. In a system with long-range interactions, information about the quench is expected to reach distant spins immediately.

proportional to the time. Finally, a fixed value (saturation) is achieved. We provide a full analytical description of the correlation dynamics. Consequently, we find the time needed to achieve some given correlation value at a given distance r and thus establish analytical formulas for the propagation of correlations. We show that the correlation dynamics changes from $r(t) \propto t^{1/\mu}$ to $r(t) \propto t^{1/(2\mu)}$ at a certain crossover time. A special case is $\mu = 1$, where a strictly linear light cone occurs in the first (ballistic) phase of the motion. However, the continuation of the linear trend is not possible and, at a certain moment of time, the propagation changes to standard diffusion.

The article is organized as follows. In Sec. II we introduce the investigated system and the theoretical model. Next, in Sec. III we present and comment on the results of the numerical simulations of the introduced model. In Sec. IV we present the results of the analytical approach in the central spin approximation. Finally, in Sec. V we summarize and conclude the work.

II. MODEL

In this section we introduce the system under study and the physical model. We also present the numerical and analytical methods used to obtain the results.

The system is a chain of N spins (chosen to be odd for convenience) distributed on a regular lattice with unit lattice constant and periodic boundary conditions. In this system we consider a local quench leading to a single quasiparticle moving along the chain in both directions (see Fig. 1). The Hamiltonian has the form

$$H = J\left(\frac{1}{2}\sum_{\alpha}\epsilon_\alpha\left(1-\hat{\sigma}_z^\alpha\right)+\sum_{\alpha,\beta}V_{\alpha\beta}\hat{\sigma}_+^\alpha\hat{\sigma}_-^\beta\right), \tag{1}$$

where $\sigma_\pm^\alpha = (\sigma_x^\alpha \pm i\sigma_y^\alpha)/2$, and σ_i^α, $i = x, y, z$ are Pauli matrices acting on spin α. Here, J sets the overall energy scale, $J\epsilon_\alpha$ is the on-site energy, and $JV_{\alpha\beta}$ is the coupling between spins α and β. To simplify the notation, we will scale the time into units of $\hbar/J$, which technically corresponds to setting $J = \hbar = 1$.

Dimensionless energies ϵ_α (in units of J) are uncorrelated random variables uniformly distributed on the interval $[-W/2, W/2]$, where the parameter W determines the strength of the disorder. The interspin coupling $V_{\alpha\beta}$ has a power-law character,

$$V_{\alpha\beta} = \begin{cases} \frac{1}{|\alpha-\beta|^\mu} & \text{for} \quad \alpha \neq \beta, \\ 0 & \text{for} \quad \alpha = \beta, \end{cases} \tag{2}$$

where $|\alpha - \beta|$ is the distance between the spins α and β.

Initially, the system is in the fully polarized state,

$$|\text{ini}\rangle = |\underbrace{\uparrow\uparrow \ldots \uparrow}_{N}\rangle, \tag{3}$$

i.e., there are no correlations between the spins.

The central spin ($\alpha = 0$) is then flipped (local quench). This leads to the spreading of the single-spin excitation through the system carrying the information about the quench to distant atoms. Quantitatively, the correlation between spin α and the initially quenched one is given by the two-point correlation function, which can be measured in experiments,

$$C_\alpha(t) = \left\langle \langle \hat{\sigma}_z^\alpha(t)\hat{\sigma}_z^0(t)\rangle - \langle \hat{\sigma}_z^\alpha(t)\rangle\langle \hat{\sigma}_z^0(t)\rangle \right\rangle_{\text{dis.}}, \tag{4}$$

where $\langle \ldots \rangle_{\text{dis}}$ stands for the average over disorder realizations, and $\langle \ldots \rangle$ denotes the quantum mechanical average. The state vector is given by

$$|\Psi\rangle = \sum_\alpha a_\alpha(t)|\alpha\rangle, \quad |\alpha\rangle = \hat{\sigma}_-^\alpha|\text{ini}\rangle, \tag{5}$$

where $a_\alpha(t)$ are time-dependent coefficients of expansion of the system into a basis of states localized at a site. The operator $\hat{\sigma}_z^\alpha$ acts on the localized basis state according to

$$\hat{\sigma}_z^\alpha|\beta\rangle = \begin{cases} +|\beta\rangle & \text{for} \quad \alpha \neq \beta, \\ -|\beta\rangle & \text{for} \quad \alpha = \beta. \end{cases} \tag{6}$$

Using Eqs. (4), (5), and (6), it is straightforward to see that

$$C_\alpha(t) = \begin{cases} \langle 4|a_0(t)|^2|a_\alpha(t)|^2\rangle_{\text{dis.}} & \text{for} \quad \alpha \neq 0, \\ -\langle 4|a_0(t)|^2(1-|a_0(t)|^2)\rangle_{\text{dis.}} & \text{for} \quad \alpha = 0. \end{cases} \tag{7}$$

As seen here, the correlation function can be expressed by the occupations of the involved sites. We find the time evolution of the occupations by the exact numerical diagonalization of the Hamiltonian (1), which allows us to compute the correlation function $C_\alpha(t)$ using Eq. (7). Simulations were performed for 25 million disorder realizations. We took advantage of periodic boundary conditions by obtaining N realizations of disorder from a single diagonalization by arbitrarily choosing the initially rotated spin.

As an alternative to the correlation function, we could consider the entanglement entropy dynamics of one spin with the rest of the system. We present this approach in Appendix A.

III. NUMERICAL RESULTS

In this section we present the results obtained by a numerical solution of the model described in Sec. II.

A. Time evolution of correlations

Figure 2 shows the correlation map for the system of $N = 1001$ spins and disorder strength $W = 200$ as a function

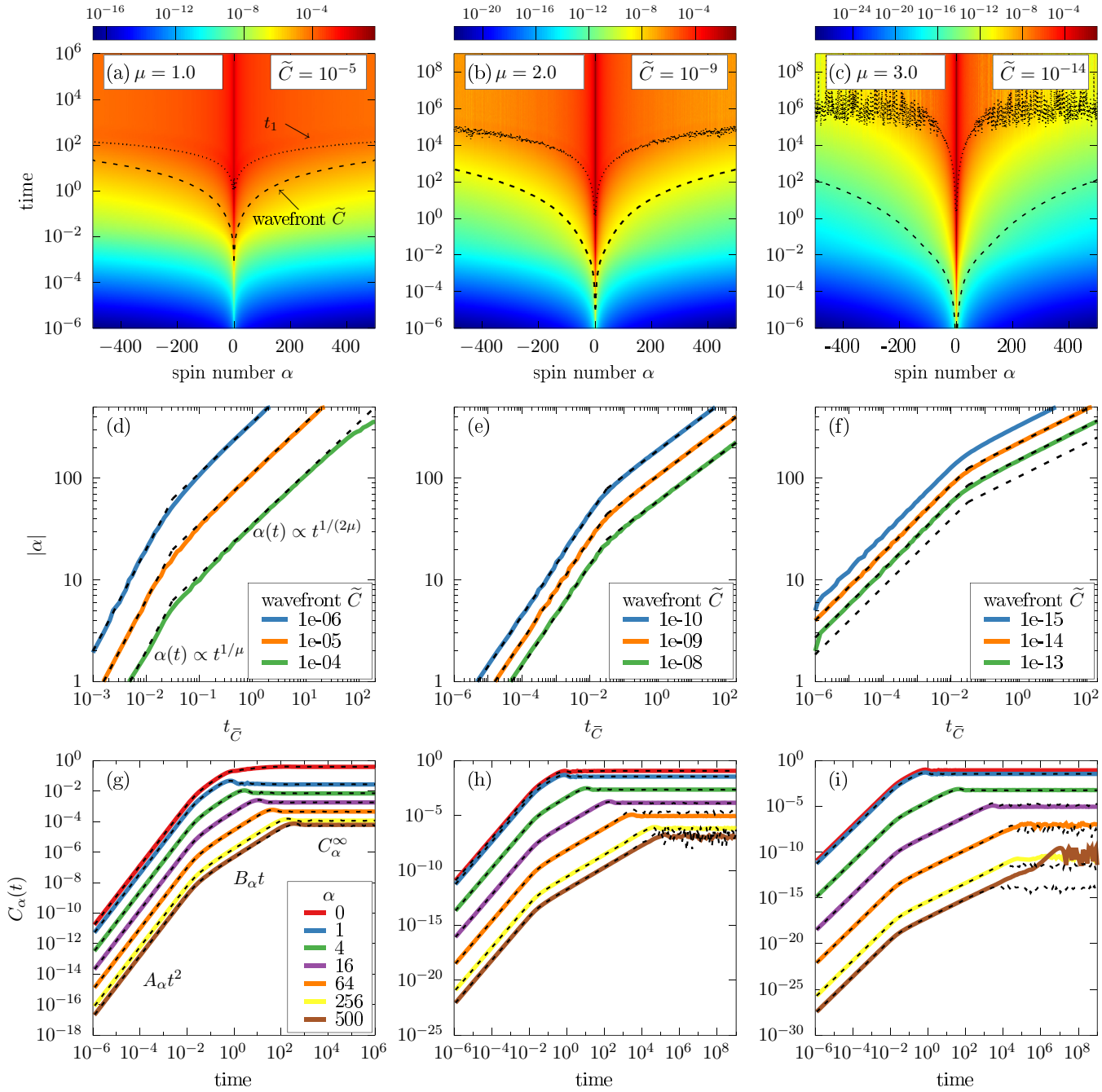

FIG. 2. (a)–(c) Map of time evolution of the absolute value of the correlation function $|C_\alpha(t)|$ [Eq. (4)] for every single node in the system of $N = 1001$ spins with disorder strength $W = 200$. Color maps indicate the values of the correlation function as a function of the spin number and time for three different values of the interaction exponent ($\mu = 1.0,\ 2.0,\ 3.0$). The dashed lines indicate the propagation fronts defined by $C_\alpha(t) = \widetilde{C}$ (with $\widetilde{C}$ given in the upper-right corner of each subfigure). The same correlation fronts are shown again in log-log scale in subfigures [(d)–(f)], where dashed lines represent analytical results obtained by employing central spin model (see Sec. III B), and the axes have been swapped to better represent the propagation of the correlation. Additionally, in panels [(a)–(c)] we represent by dotted line the light cone region given by the time t_1 [see Fig. 3(e) and Eq. (29)], outside which correlations diminish much faster (but still power law) than inside the cone [see Figs. 3(a)–3(c), and Eqs. (24), (26), and (28)]. (g)–(i) Correlation function $|C_\alpha(t)|$ as a function of time for spins $\alpha = 0,\ 1,\ 4,\ 16,\ 64,\ 256,\ 500$. Dashed lines here indicate the numerical solution of the central spin model, where simulations were performed for 500 000 disorder realizations.

of time for selected exponent values $\mu = 1.0,\ 2.0,\ 3.0$. One can see that the correlations increase with time and saturate at a certain level after a certain time, which increases with the node number. We do not observe any decay of the correlations at longer times. From the correlation dynamics for individual spins, we find the propagation front for a predefined correlation value $\widetilde{C}$, i.e., a curve in the $\alpha - t$ plane representing the times t at which the correlation at the node α reaches the value $\widetilde{C}$. These fronts are indicated in Figs. 2(a)–2(c) by the dashed lines for the indicated correlation value. They are also

depicted in Figs. 2(d)–2(f), where one can see their power-law nature, changing, however, towards a decreasing exponent at a certain node number. The choice of $\widetilde{C}$ is subject to significant constraints. It has to be less than the minimum saturation value of $C_\alpha(t)$ (for spins far from the center, $\alpha \gg 1$). For meaningful results, it has to exceed the maximal correlation value at the first time step of the simulation (for spins close to the center, $\alpha \simeq 1$). Thus there is a very narrow range of $\widetilde{C}$ for which this is satisfied. In addition, as the exponent μ increases, which is equivalent to a decreasing coupling range, the system becomes less and less correlated and the range of useful values of $\widetilde{C}$ shifts toward very small magnitudes [see Figs. 2(c) and 2(f)]. As long as saturation has not been reached, the selected value of $\widetilde{C}$ merely scales the time dependence.

Tracing the correlation front yields significant information about the evolution of the system. However, on both sides of the border defined by the arbitrary value of $\widetilde{C}$, the decay of correlations follows the same power law; hence this approach does not establish the light cone as it was defined in the Introduction. An alternative method can be proposed using analytical formulas, as discussed in Sec. IV C.

To better understand the correlation dynamics, in Figs. 2(g)–2(i) we show the time dependence of the correlation for a few nodes ($\alpha = 0,\ 1,\ 4,\ 16,\ 64,\ 256,\ 500$). For a strong disorder, the increase in correlation occurs qualitatively in the same way for each spin, namely, one observes three phases of dynamics.

At first the correlations increase as a quadratic function of time,

$$C_\alpha(t) = A_\alpha t^2, \quad \text{for } t < t_0^{(\alpha)}, \tag{8}$$

where A_α is the appropriate proportionality factor. This $\propto t^2$ evolution is a fundamental property of quantum systems with a coupling diminishing according to a power law with respect to distance, derived from the short-time perturbation theory (see, e.g., Ref. [25]). Then, at a certain crossover time $t_0^{(\alpha)}$, the time dependence changes to linear,

$$C_\alpha(t) = B_\alpha t, \quad \text{for } t_0^{(\alpha)} < t < t_1^{(\alpha)}, \tag{9}$$

with B_α as proportionality factor. Finally, at $t = t_1^{(\alpha)}$ the correlator reaches a constant value (saturates),

$$C_\alpha(t) = C_\alpha^\infty, \quad \text{for } t_1^{(\alpha)} < t. \tag{10}$$

From the condition of continuity of $C_\alpha(t)$ the crossover times can be expressed by

$$t_0^{(\alpha)} = B_\alpha / A_\alpha \tag{11}$$

and

$$t_1^{(\alpha)} = C_\alpha^\infty / B_\alpha. \tag{12}$$

The same dynamics was observed for the mean-squared displacement of a single excitation in the same model (for $\mu = 1$) presented in Ref. [26].

We found the dependence of the dynamical parameters on the site index by fitting power-law functions to the subsequent regimes of correlation dynamics described by Eqs. (8)–(10). The dynamical parameters A_α, B_α, and C_α^∞ appear to be power-law functions of the distance $|\alpha|$ with integer or rational exponents. Both A_α and B_α are inversely proportional to $|\alpha|^{2\mu}$, as depicted in Figs. 3(a) and 3(b). The first crossover time $t_0^{(\alpha)} \equiv t_0$ is roughly distance independent, except for small values of $|\alpha|$ [Fig. 3(d)]. As a function of spin number, the saturation level decreases as $1/|\alpha|^\mu$ [see Fig. 3(c)]. The noise in Figs. 3(c)–3(e), apparent especially for the high magnitude of exponent μ and distant sites, comes from the unavoidably insufficient number of disorder realizations. Using a simple resonance-counting argument, one can notice that the number of spins lying at a distance $|\alpha|$ and resonant to the central spin (in the first-order approximation) is proportional to $V_{\alpha 0}/W$; hence for the considered system of $N = 1001$ spins, $W = 200$, and $\mu = 3.5$, one would need a number of disorder realizations at least on the order of 10^{11} to allow for one resonant case on average for distant nodes.

For completeness, in Appendix B we present the results for weakly disordered systems.

B. Central spin approximation

In this section we introduce the central spin approximation in which an analytic solution, approximating well the full model, becomes available [26] (see Sec. IV). When the disorder is strong, the coupling can be treated as a perturbation in the Hamiltonian. In the first-order approximation to the evolution, one includes only the couplings between all spins and the central one. Thus the information about the quench is carried directly to the distant spins without the involvement of intermediate jumps. The correlation dynamics in the central spin approximation reproduces the dynamics of the full model in the strong disorder regime. The dashed black lines in Figs. 2(g)–2(i) represent the simulation results of the central spin approximation, which perfectly match the data of the full model for short-range and moderate sites, although it reveals a discrepancy for distant sites. However, this can be considered as a numerical error coming from too few disorder realizations, as explained above. We discuss the limits of applicability of the central spin approximation in Appendix C.

IV. APPROXIMATE ANALYTICAL SOLUTION

The central atom model allows us to find analytical expressions for the correlation function and dynamical parameters by using the theory presented in Ref. [26]. Here we present a more straightforward approach that leads to the same analytical formulas. We find analytical expressions for the correlation function, the dynamic parameters as a function of the distance from the central spin, the disorder strength, and the exponent μ. This allows us to find the time of reaching a given value of correlation for a given spin and determine the existence of the light cone in the model.

In the high-disorder regime, the survival occupation of the central site $|a_0(t)|^2 \approx 1$. We can then write the approximate formula for the correlator (7)

$$C_\alpha(t) = 4\langle |a_\alpha(t)|^2 \rangle_{\text{dis.}} \quad \text{for} \quad W \gg 1, \quad \alpha \neq 0. \tag{13}$$

A. Solution of two-spin model

Since only direct jumps from the central site to distant ones are important (central spin model) in the leading order,

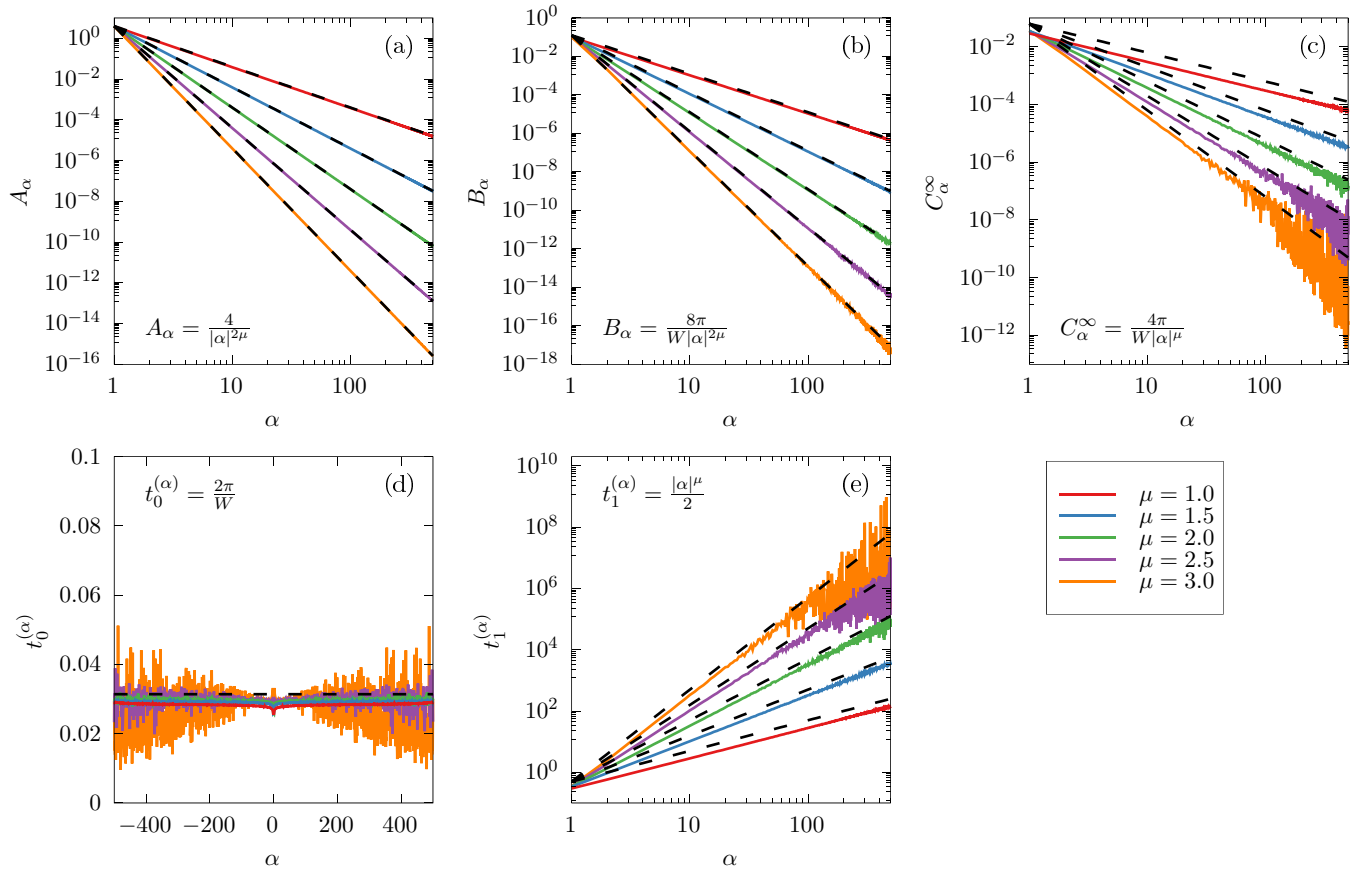

FIG. 3. Parameters of the evolution of correlations as a function of the distance from the central spin for several values of the exponent $\mu = 1.0,\ 1.5,\ 2.0,\ 2.5,\ 3.0$. In each subfigure, black dashed lines indicate the results obtained from the approximate analytical solution (see Sec. IV), described by formulas given in the panels. (a) Proportionality factor A_α for the quadratic regime, see Eq. (8); (b) proportionality factor B_α for the linear regime, see Eq. (9); (c) saturation level C_α^∞, see Eq. (10); (d) crossover time $t_0^{(\alpha)}$ between quadratic and linear regime; and (e) crossover time $t_1^{(\alpha)}$ between linear and saturating regime.

one can neglect also the presence of other spins to accurately calculate the occupation of the distant site. Let us now find these occupations of the individual sites assuming a two-spin model. One considers a system consisting of only two spins, that is, the central one and the one with index α. The Hamiltonian corresponding to the system having two spins of uniformly distributed on-site energies ϵ_0 and $\epsilon_\alpha = \epsilon_0 + \epsilon$ has the matrix form of

$$H = \left(\epsilon_0 + \frac{1}{2}\epsilon\right)\mathbb{I} + \frac{1}{2}\begin{pmatrix} -\epsilon & 2V_\alpha \\ 2V_\alpha & \epsilon \end{pmatrix}, \tag{14}$$

where $\mathbb{I}$ is 2×2 unit matrix and $V_\alpha = 1/|\alpha|^\mu$ is the coupling to the αth spin. One can easily diagonalize the above Hamiltonian. The eigenenergies $E_\pm$ and the corresponding eigenvectors $u_\pm$ are

$$E_\pm = \epsilon_0 + \frac{1}{2}\epsilon \pm \frac{1}{2}\Omega, \tag{15}$$

$$u_+ = \begin{pmatrix} \sin(\theta/2) \\ \cos(\theta/2) \end{pmatrix}, \quad u_- = \begin{pmatrix} \cos(\theta/2) \\ -\sin(\theta/2) \end{pmatrix}, \tag{16}$$

where we denote $\Omega = \sqrt{\epsilon^2 + 4V_\alpha^2}$, $\epsilon = \Omega\cos\theta$, and $2V_\alpha = \Omega\sin\theta$. Then the time evolution of the amplitude of probability for spin α is given by

$$a_\alpha(t) = \langle\alpha|\Psi(t)\rangle = \langle\alpha|e^{-iHt}|0\rangle = \sum_{n=\pm}\langle\alpha|n\rangle\langle n|0\rangle e^{-iE_n t}. \tag{17}$$

Combining Eqs. (13), (15), (16), and (17), we get

$$C_\alpha(t) = 4V_\alpha^2\left\langle\frac{\sin^2(\Omega t/2)}{(\Omega/2)^2}\right\rangle_{\text{dis.}}. \tag{18}$$

The average over disorder realizations can be obtained by integration with the probability density function of ϵ. Since ϵ is a difference between two uniformly distributed random variables on an interval $[-W/2, W/2]$, its probability density function is the triangle function

$$f_0(\epsilon) = \begin{cases} (W - |\epsilon|)/W^2, & \epsilon \in [-W, W]; \\ 0, & \text{otherwise.} \end{cases} \tag{19}$$

Then the correlation is

$$C_\alpha(t) = 4V_\alpha^2\int_{-W}^{W} d\epsilon\, f_0(\epsilon)\frac{\sin^2[\Omega(\epsilon)t/2]}{[\Omega(\epsilon)/2]^2}. \tag{20}$$

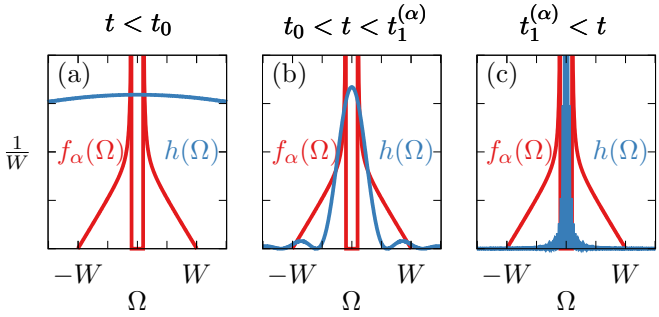

FIG. 4. Schematic plot of the probability distribution of eigenenergies separation: (a) for the first phase of motion [$C_\alpha(t) \propto t^2$]; (b) for the second phase of motion [$C_\alpha(t) \propto t$]; and (c) for the saturation phase [$C_\alpha(t) = C_\alpha^\infty$].

By changing the integration variable to Ω, we obtain

$$C_\alpha(t) = 4V_\alpha^2 \int d\Omega f_\alpha(\Omega) \frac{\sin^2(\Omega t/2)}{(\Omega/2)^2}, \tag{21}$$

where

$$f_\alpha(\Omega) = f_0(\sqrt{\Omega^2 - 4V_\alpha^2}) \frac{|\Omega|}{\sqrt{\Omega^2 - 4V_\alpha^2}} \tag{22}$$

is the probability density function of Ω for a given spin α, i.e., it depends on the distance from the origin of the system. When W and $|\alpha|$ increase, $f_\alpha(\Omega)$ tends to $f_0(\epsilon)$.

B. Triple phase dynamics

This allows us to explain the triple-phase dynamics of the correlation growth. First, for very short timescales the function $h(\Omega) = \sin^2(\Omega t/2)/(\Omega/2)^2$ in Eqs. (18), (20), (21) can be approximated as $h(\Omega) \approx t^2$, and the integral of the probability density function is equal to unity [see Fig. 4(a)]. The correlator then follows the form

$$C_\alpha(t) = \frac{4t^2}{|\alpha|^{2\mu}}. \tag{23}$$

Then, according to Eq. (8), the first dynamical parameter is

$$A_\alpha = \frac{4}{|\alpha|^{2\mu}}, \tag{24}$$

which is sketched by the dashed lines in Fig. 3(a) and perfectly matches the numerical data.

Next, for moderate times $t_0 < t < t_1$ [Fig. 4(b)], the function $h(\Omega)$ probes the central part of the distribution but is still relatively broad and therefore insensitive to the narrow central gap (especially for remote nodes). For increasing time, $h(\Omega)$ tends to be proportional to un-normalized Dirac delta of area of $2\pi t$. More specifically, the width of $h(\Omega)$ decreases as $1/t$. The time it takes for the peak of $h(\Omega)$ to be inside the gap is proportional to $1/V_\alpha$ (the width of the gap). This time gets larger as $|\alpha|$ increases, and hence the third phase of motion [Eq. (10)] starts later for high $|\alpha|$. In contrast, the width of the distribution of $f_\alpha(\Omega)$ is large. Thus, $h(\Omega)$ explores the narrow region around the even narrower gap of $f_\alpha(\Omega)$ at $1/W$ (top of the distribution function). Therefore, the integral over Ω is approximately equal to the area under $h(\Omega)$ multiplied by $1/W$, and Eq. (21) takes the form

$$C_\alpha(t) \approx 4|V_{\alpha 0}|^2 \int_{-\infty}^{\infty} d\Omega f_0(\Omega) 2\pi t \delta(\Omega) = \frac{8\pi}{W|\alpha|^{2\mu}} t, \tag{25}$$

where, according to Eq. (9), the second parameter is

$$B_\alpha = \frac{8\pi}{W|\alpha|^{2\mu}}, \tag{26}$$

which perfectly fits the data in Fig. 3(b).

From the requirement of continuity, Eq. (11), the crossover time between the first and second phases is

$$t_0 = \frac{2\pi}{W} \tag{27}$$

and is the same for all sites.

Finally, we obtain the saturation level. When the function $h(\Omega)$ becomes narrow, its peak coincides with the gap inside the distribution $f_\alpha(\Omega)$ [Fig. 4(c)]. Then the peak does not contribute and only the oscillating tail has a contribution to the integral. We approximate $h(\Omega) \approx \frac{1/2}{(\Omega/2)^2}$, taking the average of the rapidly varying sine-squared function in the numerator. Then the saturation of the correlation is

$$\begin{aligned} C_\alpha^\infty &= 8 \int_{2V_r}^{\sqrt{W^2+4V_\alpha^2}} d\Omega f_\alpha(\Omega) \frac{1/2}{(\Omega/2)^2} \\ &= \frac{4\pi}{W|\alpha|^\mu} \arctan(W|\alpha|^\mu) - \frac{8}{W|\alpha|^{2\mu}} \ln\left[1 + \left(\frac{W|\alpha|^\mu}{2}\right)^2\right] \\ &\approx \frac{4\pi}{W|\alpha|^\mu}, \end{aligned} \tag{28}$$

where the approximate result was obtained by taking $\arctan(x) \approx \pi/2$ for $x \gg 1$ and by neglecting the second-order terms in V_α/W. The analytical formula from Eq. (28), with dashed lines marked in Fig. 3(c), overestimates the numerical results. However, the deviation from the numerical data decreases as the exponent μ increases. This discrepancy may be caused by the inaccuracy of the approximation done in Eq. (13), where we assumed the occupation of the central spin, $|a_0(t)|^2$, close to unity. The asymptotic survival probability, $|a_0(\infty)|^2$, can actually subtly but not marginally deviate from unity, the less the higher μ is. Then the approximation in Eq. (18) is more accurate if the exponent μ is large. However, for each value of μ we consider, the survival probability is departed enough from unity to cause the deviation seen in Fig. 3(c).

From the second continuity relation in Eq. (12) we get the second crossover time,

$$t_1 = \frac{|\alpha|^\mu}{2}. \tag{29}$$

The above derivations explain the origin of the triple dynamics and find the correct values for the dynamical parameters.

C. Speed of propagation—Derivation of the light cone

Now we want to extract the speed of propagation of the correlation from the above derivations. For this purpose we will find the time at which the given spin reaches a certain

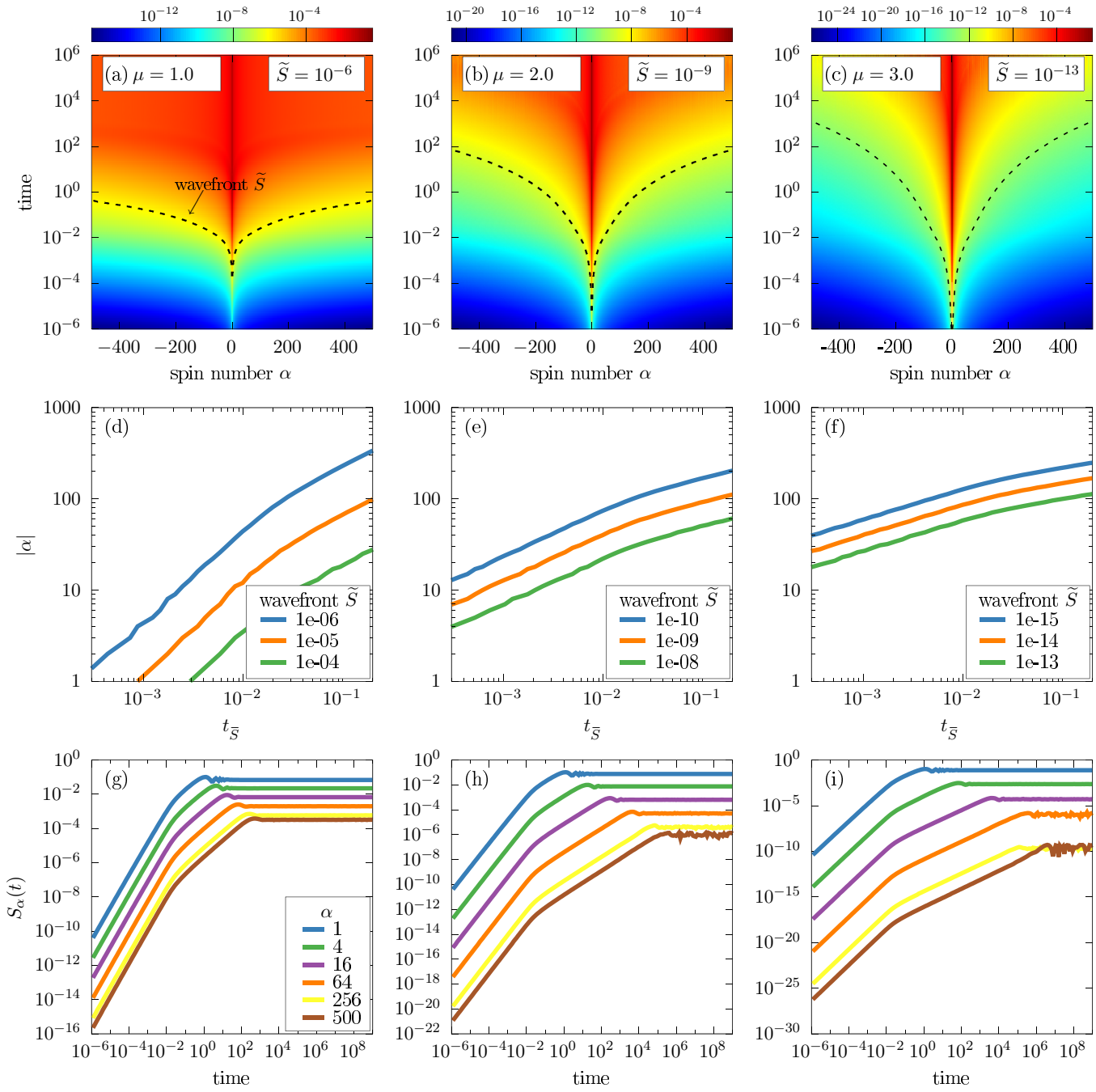

FIG. 5. (a)–(c) Map of time evolution of the entanglement entropy $S_\alpha(t)$ [Eq. (A4)] for every single node in the system of $N = 1001$ spins with disorder strength $W = 200$. Color maps indicate the values of the entropy as a function of the site number and time for three different values of the interaction exponent ($\mu = 1.0,\ 2.0,\ 3.0$). The dashed lines indicate the propagation fronts defined by $S_\alpha(t) = \widetilde{S}$ (with $\widetilde{S}$ given in the upper-right corner). The same correlation fronts are shown again in log-log scale in subfigures (d)–(f), and the axes have been swapped to better represent the propagation of the correlation. (g)–(i) Entanglement entropy $S_\alpha(t)$ as a function of time for spins $\alpha = 1,\ 4,\ 16,\ 64,\ 256,\ 500$.

value of the correlation $\widetilde{C}$. The way the wave front evolves over time determines the shape of the light "cone."

The result depends on which phase of the dynamics $\widetilde{C}$ is in for a particular spin. Thus if $\widetilde{C}$ is in the first (quadratic) phase [Eq. (8)], the time required to reach such a correlation is

$$t_{\widetilde{C}} = \frac{\sqrt{\widetilde{C}}}{2}|\alpha|^{\mu}, \tag{30}$$

which has to be less than t_0. On the other hand, if $\widetilde{C}$ is in the second (linear) phase [Eq. (9)], the time to reach this correlation value is

$$t_{\widetilde{C}} = \frac{W\widetilde{C}}{8\pi}|\alpha|^{2\mu}. \tag{31}$$

These dependencies are sketched by the dashed lines in Figs. 2(d)–2(f) and perfectly match the numerical data. On

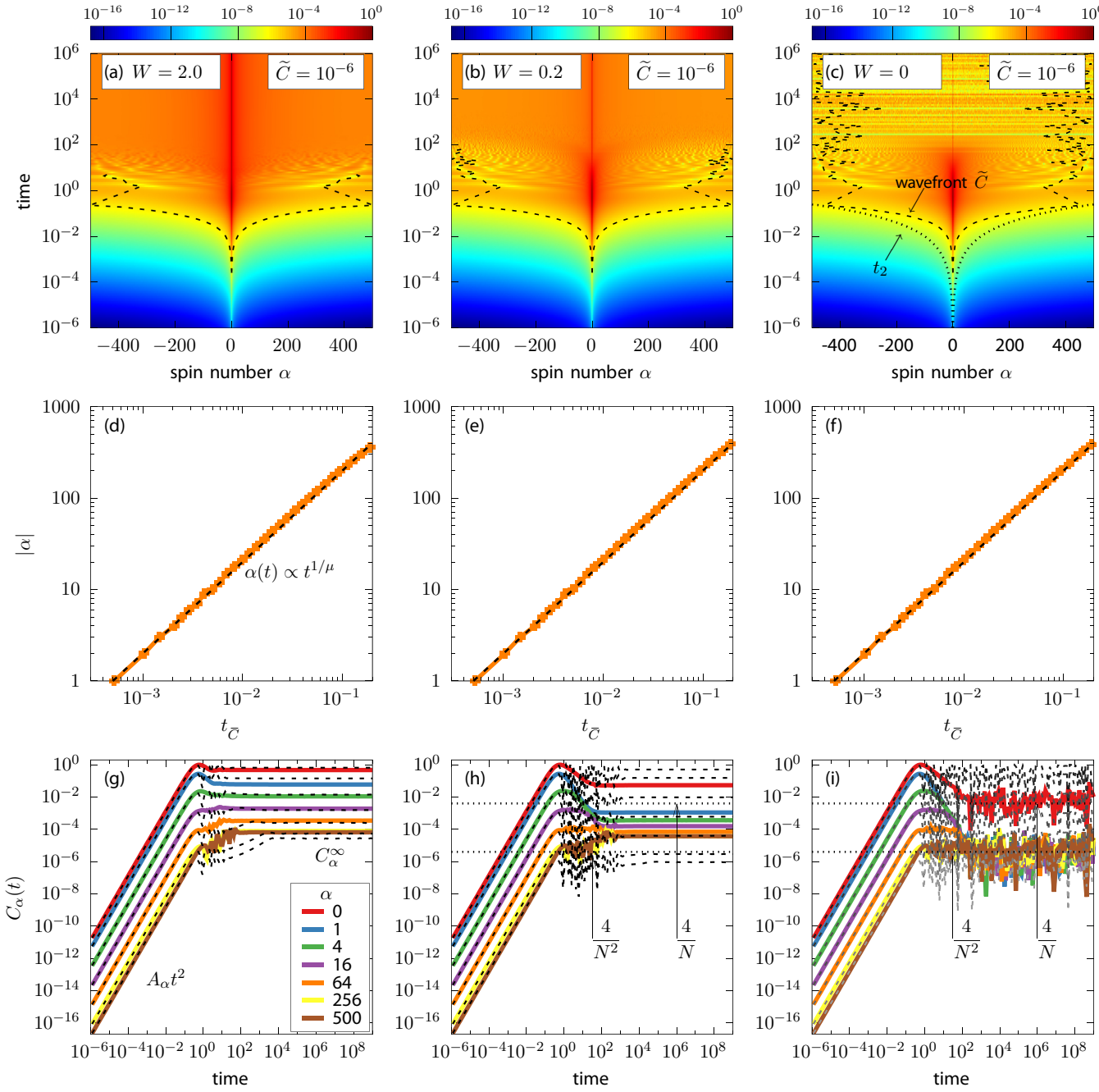

FIG. 6. (a)–(c) Map of time evolution of the absolute value of the correlation function $|C_\alpha(t)|$ [Eq. (4), cf. Fig. 2] for every single node in the system of $N = 1001$ spins, coupling exponent $\mu = 1$, and for three different values of the disorder strength, $W = 2,\ 0.2,\ 0$. The dashed lines indicate the propagation fronts defined by $C_\alpha(t) = \widetilde{C}$ (with $\widetilde{C}$ given in the upper-right corner of each subfigure). The same correlation fronts are shown again in log-log scale in subfigures (d)–(f), where dashed lines represent analytical result obtained in Sec. IV [see. Eq. (30)], and the axes have been swapped to better represent the propagation of the correlation. (g)–(i) Correlation function $|C_\alpha(t)|$ as a function of time for spins $\alpha = 0,\ 1,\ 4,\ 16,\ 64,\ 256,\ 500$. The dashed lines here indicate the numerical solution of the central spin model where simulations were performed for 500 000 disorder realizations. The dotted lines in (h) and (i) indicate limit values of correlation functions $C_0(\infty)$ and $|C_\alpha(\infty)|$ (the same for all α) in the disorder-free system [cf. Eq. (B1)].

a doubly logarithmic scale, these are straight lines indicating the power-law dependencies.

The character of the propagation changes with time. In the first phase $|\alpha(t)| \propto t^{1/\mu}$, while in the second phase the dynamics slows down, and $|\alpha(t)| \propto t^{1/2\mu}$.

The limiting time between the two regimes is t_0, which is independent of the choice of node number or the power-law exponent, so regardless of the choice of $\widetilde{C}$, the crossover will be observed at the same point (dependent only on the strength of the disorder). In the special case of $\mu = 1$, the wave-front

propagation in the first phase is ballistic, with the velocity $2/\sqrt{\tilde{C}}$ [or $2J/(\hbar\sqrt{\tilde{C}})$ in physical time units], which depends on the choice of the threshold value but is independent of the disorder strength. This is also a velocity at which a small perturbation of the system's ground state would propagate.

The definition of a cone presented here can be problematic, because the delineated cone does not demarcate the area beyond which the decay of correlations becomes faster. An alternative definition of the light cone may be based on the fact that in the saturation region the spatial decay of correlations is faster than outside this region [see Figs. 3(a)–3(c)]. Therefore it seems sensible to determine the cone as a line in time and distance separating the saturation area from the other phases. The analytic form of the cone comes straightforwardly from Eq. (29),

$$\alpha(t) = (2t)^{1/\mu}. \tag{32}$$

The above formula allows one to determine the speed of propagation of the correlation. In the particular case $\mu = 1$, when above relation is strictly linear, the corresponding velocity of propagation is equal to 2 (or $2J/\hbar$ in physical time units). For $\mu > 1$ the dynamics remains always sub-ballistic.

V. DISCUSSION

The propagation of correlations calculated in Sec. IV C varies depending on whether the given correlation value is within the first or second phase of the dynamics. This means that the character of propagation changes depending on the phase of the dynamics. This can be clearly seen in Figs. 2(d)–2(f), where the time to reach a given correlation level $\tilde{C}$ is shown as a function of the distance from the center of the chain. One can see the change in the slope of the trend from a certain distance. Initial ballistic motion [$\alpha(t) \propto t$] for $\mu = 1$ changes to standard diffusion [$\alpha(t) \propto \sqrt{t}$]. Ballistic motion implies the existence of a linear light cone, that is, a constant propagation velocity. For $\mu > 1$, one can think of a sublinear "cone."

One can also ask whether the finite size of the system plays any role. It is particularly concerning for the case of $\mu = 1$, where the saturation level of the correlation (and thus the occupation of the site) decreases as $1/|\alpha|$. Therefore the sum of occupations is divergent, and thus one may expect the model to break down at some point. However, in the thermodynamic limit the saturation phase for very far spins begins at infinite times since $t_1 \propto r \to \infty$. The infinite t_1 implies that the occupation cannot saturate and remains in the second phase of evolution [Eq. (9)], which diminishes as $1/|\alpha|^2$ and the corresponding sum of occupations is convergent.

VI. CONCLUSIONS

We investigated the propagation of correlations in a spin chain after a single local quench in the presence of large disorder and long-range couplings. The main feature observed in the system is the triple-phase evolution of correlation at each site, which results in a change in the propagation trend of the correlation front. The "light cone" in the strongly disordered system can be strictly linear only in the particular case of $\mu = 1$ and only as long as the correlation is in the first phase of motion. For $\mu > 1$ the propagation is sub-ballistic in the first phase and becomes subdiffusive in the second phase of motion. All effects observed in the numerical simulations are explained by an analytical model that describes the transfer of correlations directly from the initially quenched spin to distant spins bypassing the intermediate sites.

ACKNOWLEDGMENTS

Calculations have been partially carried out using resources provided by the Wroclaw Centre for Networking and Supercomputing [27], Grant No. 203.

APPENDIX A: ENTANGLEMENT ENTROPY

In this Appendix we show that the propagation of correlations can also be considered in terms of von Neumann entropy, which is a measure of quantum information in a system. In doing so we search for the degree of entanglement between some node α and the rest of the chain. For this we use the von Neumann entanglement entropy, defined as

$$S = -\mathrm{Tr}\rho \ln \rho, \tag{A1}$$

where $\rho = |\Psi\rangle\langle\Psi|$ is the density matrix of the system, and the state of the system can be expressed in the localized state basis [cf. Eq. (5)],

$$|\Psi\rangle = \sum_{\beta} a_\beta(t)|\beta\rangle. \tag{A2}$$

As a next step we perform the Schmidt decomposition of the state:

$$\begin{aligned}|\Psi\rangle &= a_\alpha(t)|\uparrow \ldots \uparrow\rangle_{\beta\neq\alpha} \otimes |\downarrow\rangle_\alpha \\ &\quad + \sum_{\beta\neq\alpha} a_\beta(t)|\uparrow \ldots \downarrow \ldots \uparrow\rangle_{\beta\neq\alpha} \otimes |\uparrow\rangle_\alpha \\ &= a_\alpha(t)|\uparrow \ldots \uparrow\rangle_{\beta\neq\alpha} \otimes |\downarrow\rangle_\alpha \\ &\quad + \sqrt{1-|a_\alpha(t)|^2}\sum_{\beta\neq\alpha} \frac{a_\beta(t)}{\sqrt{1-|a_\alpha(t)|^2}} \\ &\quad \times |\uparrow \ldots \downarrow \ldots \uparrow\rangle_{\beta\neq\alpha} \otimes |\uparrow\rangle_\alpha,\end{aligned} \tag{A3}$$

where we denote

$$|\uparrow \ldots \uparrow\rangle_{\beta\neq\alpha} = \bigotimes_{\beta\neq\alpha} |\uparrow\rangle_\beta$$

and

$$|\uparrow \ldots \downarrow \ldots \uparrow\rangle_{\beta\neq\alpha} = \bigotimes_{\gamma\neq\alpha,\beta} |\uparrow\rangle_\gamma \otimes |\downarrow\rangle_\beta.$$

We multiplied and divided the second term in (A3) by $\sqrt{1-|a_\alpha(t)|^2}$ to provide a normalization condition for Schmidt coefficients, which are a_α for the state of the subsystem of a single spin α and $\sqrt{1-|a_\alpha(t)|^2}$ for the state of the rest of the system. One can easily see that the decomposed states are orthonormal, so this is indeed a Schmidt decomposition. Finally, the von Neumann entanglement entropy takes

the form

$$S_\alpha(t) = -(1-|a_\alpha(t)|^2)\ln(1-|a_\alpha(t)|^2) - |a_\alpha(t)|^2\ln(|a_\alpha(t)|^2) \approx |a_\alpha(t)|^2, \tag{A4}$$

where the approximate result is valid in the strong disorder regime and for $\alpha \neq 0$. It measures the entanglement of the αth node with the rest of the system. It is clear that it only depends on the occupation of the node in question. Figure 5 shows that the calculated entanglement entropy captures qualitatively the same effects as found for the correlation function (cf. Fig. 2). The increase of entanglement with time on a node also follows three phases: quadratic in time, linear in time, and saturation. The logarithmic dependence of the entropy on time does not seem to significantly affect the power-law entropy growth [Figs. 5(g)–5(f)]. Using the central spin approximation (see Sec. III B), one can perform a reasoning similar to that presented in Sec. IV and find an approximate analytical result for the entanglement entropy.

APPENDIX B: DISORDER-FREE AND LOW-DISORDER CASES

For the sake of completeness, in this Appendix we consider the limiting case of the nondisordered system and the system with moderately strong disorder. In Fig. 6 we show the results of numerical simulations of the system with small and zero disorder. It can be seen [panels (g)–(f)] that the evolution now proceeds in two phases, quadratic in time and, immediately, saturation, i.e., excluding the middle phase where for a large disorder there is a linear growth in time. As mentioned earlier in Sec. III A, the quadratic growth in time is a fundamental result in the quantum evolution of long-range coupled systems coming from the short-time perturbation theory (see Ref. [25]). The absence of the second phase can be explained by the fact that its onset time is inversely proportional to the disorder and thus large enough in the low-disorder regime that the correlation manages to saturate early.

First, in the absence of the on-site disorder, the dynamics of the system tends to uniformly distribute the occupations at the nodes, $|a_\alpha|^2 = 1/N$, for all α. The correlation function (7) then takes the form

$$C_\alpha(t\to\infty) = \begin{cases} \frac{4}{N^2}, & \text{for} \quad \alpha \neq 0, \\ -\frac{4}{N}\left(1-\frac{1}{N}\right), & \text{for} \quad \alpha = 0. \end{cases} \tag{B1}$$

However, even in the case of $W = 0.2$ and $\mu = 1$, correlation still noticeably deviates from the above formulas, which are indicated in Figs. 6(h) and 6(i) by black dashed lines. As the disorder decreases, the saturation level begins to converge to the level defined by Eq. (B1), while the central spin model begins to deviate from the simulation results of the full model [see panels (g)–(i) of Fig. 6]. In a weakly disordered system, one can see that the increase in correlation at a node starts also with a quadratic dependence in time. However, the second phase has little or no visibility, particularly for nodes close to the center. Finally, we can also find the initial time $t_2^{(\alpha)}$ of the saturation phase in the disorder-free system,

$$t_2^{(\alpha)} = \frac{|\alpha|^{2\mu}}{N^2}, \tag{B2}$$

which grows faster with distance than the second crossover time $t_1^{(\alpha)}$ in the highly disordered chain but does not necessarily exceed it (especially for $\mu < 2$).

APPENDIX C: REGIME OF VALIDITY OF THE CENTRAL SPIN APPROXIMATION

As long as the disorder is strong, it is right to use the first-order approximation of the locator expansion presented originally in the seminal paper of Anderson published in 1958 [19], which we refer to as the central spin model. Let us now consider the limits of its applicability. The central spin model is no longer valid when second- and higher-order jumps start to play a role in the evolution of the excitation. Using a simple resonance counting argument, the probability of the first-order jump is proportional to $V_{\alpha 0}/W$, while the number of second-order jumps for the transition from spin 0 to α is proportional to

$$\sum_{0<\beta<\alpha} \frac{V_{0\beta}V_{\beta\alpha}}{W^2}. \tag{C1}$$

When the above expression becomes comparable to $V_{\alpha 0}/W$, it becomes necessary to consider higher-order transitions, and the central spin model is no longer valid. The appropriate limiting value of W can be found numerically for given μ and N. For example, in the system $N = 1001$ spins, and for $\mu = 1$ the probability of second-order transitions is equal to the probability of the first-order transitions if $W \approx 15.0$, whereas for $\mu = 2$ the critical disorder is equal to $W \approx 3.32$. The central spin model remains valid in a system with weaker disorder for a higher μ value, i.e., for a weaker coupled system.

[1] E. H. Lieb and D. W. Robinson, Commun. Math. Phys. **28**, 251 (1972).

[2] D. W. Robinson, J. Aust. Math. Soc. Ser. B Appl. Math. **19**, 387 (1976).

[3] H. Bragança, M. F. Cavalcante, R. G. Pereira, and M. C. O. Aguiar, Phys. Rev. B **103**, 125152 (2021).

[4] Y. Chougale, J. Talukdar, T. Ramos, and R. Nath, Phys. Rev. A **102**, 022816 (2020).

[5] M. Cheneau, P. Barmettler, D. Poletti, M. Endres, P. Schauß, T. Fukuhara, C. Gross, I. Bloch, C. Kollath, and S. Kuhr, Nature (London) **481**, 484 (2012).

[6] T. Langen, R. Geiger, M. Kuhnert, B. Rauer, and J. Schmiedmayer, Nat. Phys. **9**, 640 (2013).

[7] S. Hild, T. Fukuhara, P. Schauß, J. Zeiher, M. Knap, E. Demler, I. Bloch, and C. Gross, Phys. Rev. Lett. **113**, 147205 (2014).

[8] P. Richerme, Z.-X. Gong, A. Lee, C. Senko, J. Smith, M. Foss-Feig, S. Michalakis, A. V. Gorshkov, and C. Monroe, Nature (London) **511**, 198 (2014).
[9] P. Jurcevic, B. P. Lanyon, P. Hauke, C. Hempel, P. Zoller, R. Blatt, and C. F. Roos, Nature (London) **511**, 202 (2014).
[10] V. Lienhard, S. de Léséleuc, D. Barredo, T. Lahaye, A. Browaeys, M. Schuler, L.-P. Henry, and A. M. Läuchli, Phys. Rev. X **8**, 021070 (2018).
[11] J. Despres, L. Villa, and L. Sanchez-Palencia, Sci. Rep. **9**, 4135 (2019).
[12] M. Carrega, J. Kim, and D. Rosa, Entropy **23**, 587 (2021).
[13] T. Kuwahara and K. Saito, Phys. Rev. X **10**, 031010 (2020).
[14] C.-F. Chen and A. Lucas, Phys. Rev. Lett. **123**, 250605 (2019).
[15] M. C. Tran, C.-F. Chen, A. Ehrenberg, A. Y. Guo, A. Deshpande, Y. Hong, Z.-X. Gong, A. V. Gorshkov, and A. Lucas, Phys. Rev. X **10**, 031009 (2020).
[16] P. Hauke and L. Tagliacozzo, Phys. Rev. Lett. **111**, 207202 (2013).
[17] J. Schachenmayer, B. P. Lanyon, C. F. Roos, and A. J. Daley, Phys. Rev. X **3**, 031015 (2013).
[18] Z. Eldredge, Z.-X. Gong, J. T. Young, A. H. Moosavian, M. Foss-Feig, and A. V. Gorshkov, Phys. Rev. Lett. **119**, 170503 (2017).
[19] P. W. Anderson, Phys. Rev. **109**, 1492 (1958).
[20] N. Mott and W. Twose, Adv. Phys. **10**, 107 (1961),.
[21] E. Abrahams, P. W. Anderson, D. C. Licciardello, and T. V. Ramakrishnan, Phys. Rev. Lett. **42**, 673 (1979).
[22] A. Rodríguez, V. A. Malyshev, G. Sierra, M. A. Martín-Delgado, J. Rodríguez-Laguna, and F. Domínguez-Adame, Phys. Rev. Lett. **90**, 027404 (2003).
[23] F. Domínguez-Adame and V. A. Malyshev, Am. J. Phys. **72**, 226 (2004).
[24] F. A. B. F. de Moura, A. V. Malyshev, M. L. Lyra, V. A. Malyshev, and F. Domínguez-Adame, Phys. Rev. B **71**, 174203 (2005).
[25] L. Colmenarez and D. J. Luitz, Phys. Rev. Research **2**, 043047 (2020).
[26] K. Kawa and P. Machnikowski, Phys. Rev. B **102**, 174203 (2020).
[27] https://www.wcss.pl/.